NUREG/CR-1526 Vol. I
ANL-80-54 Vol. I

(Distribution
Code: R7)

ARGONNE NATIONAL LABORATORY
9700 South Cass Avenue
Argonne, Illinois 60439

PHYSICS OF REACTOR SAFETY

Quarterly Report
January—March 1980

Applied Physics Division
Components Technology Division

May 1980

Previous reports in this series

ANL-79-37	January—March 1979
ANL-79-76	April—June 1979
ANL-79-98	July—September 1979
ANL-80-25	October—December 1979

Prepared for the Division of Reactor Safety Research
Office of Nuclear Regulatory Research
U. S. Nuclear Regulatory Commission
Washington, D. C. 20555
Under Interagency Agreement DOE 40-550-75

NRC FIN Nos. A2015 and A2045

TABLE OF CONTENTS

LIST OF FIGURES

LIST OF FIGURES (Contd)

PHYSICS OF REACTOR SAFETY

Quarterly Report
January-March 1980

ABSTRACT

This Quarterly progress report summarizes work done during the months of January-March 1980 in Argonne National Laboratory's Applied Physics and Components Technology Divisions for the Division of Reactor Safety Research of the U. S. Nuclear Regulatory Commission. The work in the Applied Physics Division includes reports on reactor safety modeling and assessment by members of the Reactor Safety Appraisals Section. Work on reactor core thermal-hydraulics is performed in ANL's Components Technology Division, emphasizing 3-dimensional code development for LMFBR accidents under natural convection conditions. An executive summary is provided including a statement of the findings and recommendations of the report.

FIN No.	Title
A2015	Reactor Safety Modeling and Assessment
A2045	3-D Time-dependent Code Development

EXECUTIVE SUMMARY

BIFLO routines to calculate two-phase and single-phase thermohydrodynamic conditions following the onset of boiling have been written. These routines were merged together to form an initial preliminary version of BIFLO which is undergoing further development and testing.

Efforts to develop an analytical benchmark capability for the BIFLO modeling effort have been hampered by a number of instabilities or non-convergence problems which have been discovered when COBRA-IV-I is utilized to model a hexagonal bundle containing wire wrapped pins. These problems appear to be generic problems in the COBRA-IV-I modeling. Results obtained from the implicit steady-state initialization process do not appear to be correct; properly converged steady-state solutions must be obtained by running the code in the transient mode with constant boundary conditions and using the explicit solution technique. For some cases, the full effect of the wire wrap must be prevented from being present during the implicit initialization and only introduced during the explicit "transient" in order to preclude premature failure of the solution.

Some preliminary calculations have been completed to compare results obtained from BIFLO and COBRA-IV-I to results of a steady-state non-boiling test performed at Oak Ridge National Laboratory on THORS Bundle-6A. Results obtained with BIFLO are generally encouraging. Calculations with COBRA-IV-I are still continuing to incorporate adjustments to the input data which will more closely reflect the test conditions.

A version of the COMMIX-1A program has been obtained and input data for a 19-pin hexagonal bundle is being prepared.

The effect of sodium compressiblity and steel elasticity on the rise in inlet plenum pressure occurring in an LMFBR as a result of sodium voiding has been investigated using the PTA2 Code. Calculations were made for a model of the CRBR and for a modification of this model using a shorter inlet sodium pipe to simulate a pool rather than loop design. Compressibility and elasticity effects on lower sodium slug velocity were negligible for the pool case but appreciable for the loop case. However, the effect was still small compared to the difference in lower sodium slug velocity between the pool and loop cases, which appeared to be large enough to have a considerable effect on voiding ramp rate.

Results from several transient fission gas release codes have been obtained for two transients and the results compared and interpreted in terms of model assumptions and parameters. The codes studied are the following: FRAS3, NEFIG, GRASS-SST, FASTGRASS, and FRASPAR, a parametric code. The transients considered are the HEDL FGR-39 out-of-pile experiment and a more rapid transient typical of a LOF-TOP. FRAS3 and NEFIG were found to give very similar results, with differences in modeling and parameter assumptions largely compensating. GRASS-SST and FASTGRASS gave results that were not greatly different from each other for the one comparison presented, but there were compensating effects between release from the fuel grains and from grain boundaries and edges. The releases calculated by GRASS-SST and FASTGRASS were lower than those from FRAS3 and NEFIG. The most suitable value for the GRAINM

parameter, which adjusts the gas release rate in FRASPAR, appears to vary with the nature of the transient.

In the development work of single-phase COMMIX-1A code, an option to use the implicit formulation of the energy equation has been developed and implemented in the code. The implicit energy option permits larger time step sizes and consequently reduces the computer running time. This was confirmed by rerunning the natural circulation transient simulation of the SLSF-P2 test. In addition, the cylindrical coordinate option was re-examined. It was found that no special treatment of the mass, momentum and energy equation is required in the vicinity of the origin.

In order to investigate the thermal buoyancy effects on temperature and velocity distributions in a pipe, a computer simulation of thermal-hydraulic transient in a pipe was carried out. It was observed that in thermal buoyancy dominant flows, a buoyancy force greatly alters hydraulic resistances and creates large local temperature gradients

In the development work of the two-phase COMMIX-2 code, the two procedures (i) line-by-line, and (ii) analytic rebalance technique (ART), were used to simulate the two-phase separation problem. It was observed that both of these procedures have a higher rate of convergence than the previously used cell-by-cell procedure. The Nigmatulin boiling model has been incorporated in the code. NRC standard problem #1 is now selected as the next test problem for COMMIX-2.

The BODYFIT-1, single-phase code, which uses coordinate transformation for modeling of multiply connected geometries, has now been extended to handle 3-D distorted geometry. All the necessary formulations and coding of 3-D transformed momentum and energy equations have been completed. The code has been successfully tested with a simple test case of a distorted pin inside a hexagonal duct wall. In addition, the programming of one equation (k) and two equations (k and ε) turbulence models are also completed.

I. REACTOR SAFETY MODELING AND ASSESSMENT

(A2015)

A. BIFLO Development (J. J. Sienicki)

During the past quarter, portions of BIFLO which calculate the boiling/voiding phase of a transient were written. These new routines have been merged with the previously developed preboiling portions to form an initial version of BIFLO. This initial version is undergoing further development and testing. As the precise numerical formulation of BIFLO is expected to undergo revision and/or refinement as experience is gained from testing and application of the code, we have decided to defer a detailed discussion of the BIFLO finite difference equations. However, a general discussion of the modeling approach and numerical methodology currently employed in the code will be presented below. Also, the major areas in which further development and/or study are required will be indicated.

BIFLO models a pin bundle in terms of a few axial channels which are assumed to be interconnected so that sodium is free to flow radially between adjacent channels. Although each channel might be chosen to correspond to one or more of the hexagonal coolant rings in a bundle, this particular choice is not necessary and one can readily conceive of situations (e.g., a subassembly subjected to a severe power skew) where other channel arrangements are desirable. Individual cells in the Eulerian numerical grid may be defined during the calculation as containing either single-phase liquid or a two-phase mixture. To achieve computational efficiency, distinct and different fast running Eulerian calculations of thermohydrodynamic motions are performed in two-phase and single-phase regions. This strategy of separating the two-phase and single-phase calculations was originally applied with great success to two-dimensional problems in TWOPOOL and POOL.[1] By employing equation sets and numerical methods within each region that are designed to optimize the computational efficiency within that specific region, a considerable increase in overall efficiency can be achieved over schemes which solve one general set of equations over the entire numerical grid and which must possess the capabilities to treat both two-phase and single-phase flow in multidimensional geometry.

The initial preboiling portions of BIFLO are described in detail in the preceding Quarterly Report.[2] It will be recalled that before the onset of boiling, the thermal-hydraulic conditions are calculated with the aid of the assumption that the pressure is radially uniform. The effects of radial flow are accounted for through experimentally calibrated crossflow terms which couple the interconnected axial flows. For example, the crossflow terms in the enthalpy equations represent the radial mass flowrates per unit area between adjacent channels. In general, models for the crossflow terms between single-phase channels would be expected to depend upon the local axial momenta as well as the bundle geometry.

The assumption of a radially uniform pressure permits the axial momenta to be calculated without the necessity of determining a multidimensional pressure field. Elimination of the need to determine a multidimensional pressure field permits the achievement of fast running times. The computational

efficiency, especially for problems in which pressure bondary conditions are specified, is further enhanced through the use of a new forward elimination scheme in which the axial momentum per unit volume (in channel k at axial level j and at time level n+1) $(\rho U)_{j,k}^{n+1}$ is expressed as a linear function of of the (as yet undetermined) local total bundle flowrate at axial level j

$$G_j^{n+1} .$$

$$(\rho U)_{j,k}^{n+1} = a_{j,k} + b_{j,k} G_j^{n+1} \tag{1}$$

After determining the forward elimination constants $a_{j,k}$, $b_{j,k}$, the total bundle flowrate is then obtained from the solution of a linear equation and the momenta are finally calculated by back substitution into Eq. (1).

The determination of single-phase thermal-hydraulic conditions following boiling inception is an extension of the preboiling approach described above. In particular, the basic finite difference momentum equations are similar to those written for the preboiling calculation. As before, it is assumed that the pressure field in single-phase regions is radially uniform. It is convenient to introduce a cell-edged single-phase (axial) pressure field $P_{j-1/2}$. If a single-phase cell located in channel k at axial level j is bordered both above and below by other single-phase cells, the axial pressure drop across the cell is $P_{j-1/2} - P_{j+1/2}$. However, if the cell below at j-1,k is a two-phase cell, then the axial pressure drop is assumed to be given by $P_{sat,j-1,k} - P_{j+1/2}$ where $P_{sat,j-1,k}$ is the two-phase saturation vapor pressure of the two-phase mixture in the cell below. Similarly, if the cell above at j+1,k is a two-phase cell, then the single-phase pressure $P_{j+1/2}$ is replaced by $P_{sat,j+1,k}$. In this manner, the two-phase regions act as a source of pressure applied to the single-phase regions. It should be noted that the present approach differs fundamentally from analyses which treat the boiling region as a blockage.

The single-phase momenta are again obtained using our forward elimination approach. However, because of the presence of two-phase regions, a forward elimination involving only the local flowrate is insufficient to determine a solution. The momentum is now expressed as a linear function of the lower and upper pressures as well as the flowrate

$$(\rho U)_{j,k}^{n+1} = a_{j,k} + b_{j,k} G_j^{n+1} + c_{j,k} P_{j-1/2}^{n+1} + d_{j,k} P_{j+1/2}^{n+1} \tag{2}$$

where G_j^{n+1} is the total flowrate in all of the single-phase channels at axial level j. Applying the assumption that the single-phase pressure is radially uniform to a linearized formulation of the single-phase momentum equation together with the definition of the total flowrate yields four sets of linear equations which are solved for the forward elimination constants in Eq. (2). Substituting the representation given by Eq. (2) into the momentum equation

for particular single-phase channel, we obtain a linear equation relating the axial single-phase pressure drop $P^{n+1}_{j-1/2} - P^{n+1}_{j+1/2}$ to $P^{n+1}_{j-1/2}$, $P^{n+1}_{j+1/2}$, G^{n+1}_{j}. This equation is used to express G^{n+1}_{j} as a linear function of $P^{n+1}_{j-1/2}$, $P^{n+1}_{j+1/2}$. Combining this equation for G^{n+1}_{j} together with a second equation expressing conservation of mass within the bundle (which is dependent upon results of the two-phase calculations) results in a tridiagonal linear equation for the single-phase pressure field. After solving this one dimensional pressure equation, the single-phase flowrates and momenta are successively calculated by back substitution.

The geometrical configuration of the single-phase and two-phase regions may be fairly general with the only restriction being that all of the single-phase cells at each axial level must be interconnected. (For example, if the channels were to represent hexagonal coolant rings, then a situation where a two-phase ring would be sandwiched between two single-phase rings would be prohibited.) When applied to the calculation of a preboiling transient, the new extension of the forward elimination approach was found to be only slightly less efficient than the specialized solution of the preboiling momentum equations which required the calculation of fewer (two) forward elimination constants per cell and did not need to solve a tridiagonal system to determine the pressure field.

We now consider the formulation of the single-phase enthalpy equations. The preboiling enthalpy equations were linearized with respect to the end of time step enthalpies giving rise to an implicit coupling between enthalpies in all of the interconnected channels at the same axial level and between enthalpies in adjacent levels in the same channel. This implicit coupling permitted the use of time steps greatly exceeding the Courant condition

$$\frac{U_{j,k}\,\delta t}{\delta z_j} = 1.$$

However, to obtain a highly efficient solution, the greatly simplifying assumption that the velocity field is nonnegative was introduced. After the onset of boiling, no such assumption about the velocities can be made. The single-phase finite difference enthalpy equations used following boiling inception are similar to the equations used for the preboiling calculation. However, the coupling between enthalpies in different cells is now formulated explicitly. In particular, the terms accounting for the effects of axial convection, radial crossflow, and thermal conduction/turbulent diffusion are explicit. As a consequence of an explicit formulation of the axial convective terms, the time step sizes employed for the solution of the single-phase enthalpy equations must lie below the Courant condition limit. However, the velocity field may now be arbitrary. In the preliminary calculations performed thus far (e.g., a loss of flow transient), the explicit formulation of the crossflow and the conductive coupling between different channels, which defines an additional restriction on the time step size, has been found to yield accurate results when Courant limited time steps are used.

In two-phase regions, the fast running "TWOPOOL saturation approach"[1] is employed to calculate two-phase thermohydrodynamic motions. In this approach, sodium liquid and vapor are assumed to remain in thermodynamic equilibrium at saturation. The pressure driving the two-phase motions is therefore the saturation vapor pressure which may be expressed as a function dependent upon only one thermodynamic variable which is taken to be the liquid specific enthalpy. The liquid specific enthalpy is determined from finite difference mass and enthalpy equations for the two-phase mixture in which the terms accounting for axial and radial convection are formulated explicitly. The mass and enthalpy equations may be solved using time steps limited only by Courant condition restrictions based upon the axial and radial material velocities. This methodology achieves great computational efficiency by eliminating the need to formulate the velocities in mass/enthalpy convective terms implicitly as is characteristic of most other multidimensional two-phase numerical fluid dynamics schemes which employ similarly sized time steps. In these other schemes, such an implicit coupling is usually accomplished by solving a Poisson-like equation for the multidimensional pressure field. In our saturation approach, it is not necessary to solve such an equation and this results in much faster running times.

Axial two-phase motions are calculated by solving separate but coupled liquid and vapor momentum equations for distinct liquid and vapor velocities. This permits the modeling of high void fraction/high slip annular flow which is often achieved during sodium boiling.

Radial two-phase flow is currently calculated by solving a simplified radial momentum equation in which homogeneous (i.e., no slip) flow is assumed and terms accounting for the convection of momentum are ignored. The effects of radial friction within a bundle are modeled as in a porous medium approach.

In general, the BIFLO two-phase equations are similar to the equations modeling two-phase flow in TWOPOOL except that the semi-implicit formulation employed in TWOPOOL has been replaced by an explicit one in BIFLO.

In the preliminary calculations carried out thus far, the BIFLO two-phase methodology has performed very well using Courant limited time steps up to very high void fractions ($\alpha \lesssim 0.99$). However, it has been found that if an attempt is made to model annular flow with heat input into the thin liquid film calculated on the basis of a film conductive thermal resistance, then it may be necessary to reduce the time step to maintain a numerically stable solution as film depletion continues and the void fraction increases to still higher values ($\alpha \gtrsim 0.99$). A necessity to reduce the time step in this manner could compromise the computational efficiency of the two-phase methodology. However, beyond some calculated high void fraction (e.g., $\alpha \gtrsim 0.95$), it is usually assumed that dryout of the cladding has occurred so that the two-phase flow regime should be modeled as dispersed rather than annular. With a much reduced heat transfer coefficient modeling heat transfer to a dispersed two-phase mixture or to sodium vapor, the liquid fraction is expected to often remain of the order of 0.01 or more. While situations in which superheated vapor flow or higher void fraction two-phase flow might occur in some sodium boiling analyses, the provision to efficiently calculate such phenomena while still using large time steps limited only by a Courant condition restriction based on the material velocities has not been included in the present initial

version of BIFLO. The current modeling approach therefore assumes that as sodium vapor streaming occurs following dryout, sufficient entrainment of liquid droplets occurs to maintain a dispersed flow regime everywhere within the voided regions. Although future studies may indicate the need to incorporate additional capabilities into BIFLO (e.g., a detailed treatment of superheated vapor flow), their inclusion does not seem to be warranted at the present time.

The major problem area in BIFLO development at the present time is the proper interfacing of the two-phase and single-phase calculations. This involves the specification of fluxes for mass and enthalpy at interfaces between two-phase and single-phase regions as well as modeling of the fluid dynamical response of the single-phase regions to the two-phase pressure source. While this problem stems principally from the use of an Eulerian numerical framework in which the two-phase/single-phase interface must correspond to numerical grid cell edges, the description of interfacial phenomena is also strongly dependent upon the modeling of single-phase diversion around the two-phase regions as well as the flow regimes assumed to exist within the two-phase regions. Present attention is being devoted to the definition of the axial mass and enthalpy fluxes at two-phase/single-phase interfaces. Other aspects of the interfacing problem will be studied in the future. For example, while the current initial version of BIFLO assumes that the two-phase pressure is used in evaluating the axial pressure drop across single-phase cells which border on the top or bottom of a two-phase region, other schemes of transmitting the effects of two-phase pressurization to the single-phase regions need to be examined. In general, it is expected that considerable attention will be devoted to the interfacing of the two-phase and single-phase calculations in the future.

Another important area of ongoing study is the definition of the location of the two-phase/single-phase interface. Clearly, when the void fraction in a two-phase cell is calculated to become negative, the cell should be redefined as single-phase. A problem exists, however, in the definition of transitions from single-phase to two-phase flow. The sodium in a single-phase numerical cell located in the interior of a single-phase region is permitted to make the transition from single-phase to two-phase flow when a specified superheat criterion (which is a user defined parameter that can be taken to be zero if so desired) is exceeded. For a cell which borders on a two-phase region, the transition is always assumed to occur at zero superheat. The problem in determining the transition of numerical cells from single-phase to two-phase flow is that after the equations have been advanced over one up to several time steps, some of the cells which have just been defined as two-phase may be predicted to become single-phase again. Such cells can be calculated to undergo repetitive cycles of two-phase and single-phase behavior. These numerical fluctuations can result in the wrong effective pressure source being applied to the single-phase regions giving rise to an incorrect prediction of the voiding behavior. Therefore, the following approach is currently employed in BIFLO to determine single-phase to two-phase transitions. All cells which satisfy the appropriate thermal criteria to become two-phase are permitted to "open up." A trial time step is then calculated after which the candidate two-phase cells are examined to determine if void creation (two-phase flow) or overcompaction (an attempt to maintain single-phase flow) has occurred. If void has been created in all of the candidate cells, then the calculation is

permitted to move on to the next time step. However, if overcompaction occurs in one or more of the cells, then the time step is recalculated with only those cells in which void was created during the trial time step permitted to make the single-phase to two-phase transition. The time step is recalculated as many times as is necessary until only void creation is obtained in all of the cells which are permitted to become two-phase. This scheme has performed well in the preliminary calculations carried out thus far. However, other transition schemes are possible and one of these may provide a better definition of the two-phase region boundaries. It should be noted that in the current version of BIFLO, cells are permitted to become two-phase only when the temperature exceeds a finite or zero superheat criterion. It is thus assumed that if two-phase sodium is convected out of a boiling region into a single-phase region, then the void very rapidly collapses.

The computational efficiency of BIFLO has been considerably enhanced through the use of a multiple time step approach in which different equations are solved with different time steps. The solution of the two-phase mass, enthalpy, and momentum equations, which often model high slip/high vapor velocity conditions, is performed using a fine time step. The single-phase enthalpy and momentum equations, which usually describe the thermal-hydraulic effects of transitions, are solved with larger time steps. While the time steps used to solve the single-phase enthalpy equation must be limited by a Courant condition restriction based on the single-phase velocities, the solution of the single-phase momentum equation may be carried out with time steps greatly exceeding the Courant limit. The determination of single-phase/two-phase transitions is performed at times based on a time step consistent with the time scale over which void growth or collapse occurs. In the initial version of BIFLO, the determination of single-phase/two-phase transitions and the solution of the single-phase momentum equation are performed at the same times.

The modeling approaches and numerical methodologies which form the basis for the initial version of BIFLO permit the efficient calculation of multidimensional two-phase and single-phase thermohydrodynamic conditions in pin bundles both before and after sodium boiling inception. BIFLO development continues with special emphasis devoted to the proper interfacing of the two-phase and single-phase calculations, the definition of the two-phase region boundaries, the modeling of crossflow effects, and flow regime selection under various combinations of power and flow.

B. BIFLO Benchmarking Activities (P. L. Garner and M. F. Kennedy)

1. Convergence Problems with COBRA-IV-I

A number of instabilities or non-convergence problems have been noted during the use of the COBRA-IV-I code.[3] A discussion of these problems will be preceded by a description of the various operating modes in COBRA-IV-I.

The COBRA-IV-I code has both implicit and explicit solution techniques. The code always uses the implicit technique to initialize steady state at the beginning of a case. The solution technique used for the transient portion of a case depends on the boundary condition imposed on the flow field: the user may select either the implicit or the explicit technique if the flow field is

driven by the inlet mass flux; the explicit technique must be used when the pressure-drop boundary condition is used for the flow field.

Two types of problems have arisen while using the implicit technique to initialize steady-state solutions for problems using the geometry of the tests[4,5] run in Bundle-6A of the THORS Facility at Oak Ridge National Laboratory (ORNL). These tests were performed out-of-pile using 19 electrically heated, wire-wrapped fuel-pin simulators in a flowing sodium environment. The first type of problem was characterized by the code aborting during the implicit steady-state initialization with the messages "loss of diagonal dominance" or "out of range in properties table." This problem could be eliminated in some cases by using an option* in the code to incorporate the effect of the wire wraps into the solution over a specified number of iterations (NRAMP, user input) during implicit initialization rather than having the full effect present for the first iteration.

The second problem was the nature of the solution printed at the end of the implicit initialization (when the solution proceeded to that point): certain aspects of the solution did not appear to be truly converged. This judgement is somewhat subjective but has been checked in one way. If the solution obtained at the end of the implicit initialization has converged on steady state, then the solution should remain invariant in time when the code is run in the transient mode with boundary conditions which are fixed in time. The results obtained at the end of this "transient" have been found to be a function of the solution technique selected. If the implicit technique is used, the results at the end of a transient using constant boundary conditions are identical to the results obtained at the end of the implicit steady-state initialization. If the explicit technique is used to calculate a transient with constant boundary conditions, the solution immediately starts changing from that obtained during the implicit initialization procedure and is converging to a new steady-state solution. This new steady state is obtained after 0.25 s (250 time steps for a 19-pin geometry with 18 axial nodes) and exhibits the following differences from the implicit initialization: lateral flows differ by an order of magnitude and in direction, axial velocities differ by 20%, and temperature rises along the bundle length (on a channel basis) differ by 5%. The biggest differences are near the bundle inlet region. The solution obtained at the end of the explicit transient with constant boundary conditions appears to be a more realistic steady-state solution than that obtained using the implicit technique. This subjective judgement is motivated by the distinct repeating patterns of results which are expected for bundles of wire-wrapped pins. Tightening the convergence criteria (by more than an order of magnitude) used for the implicit technique did not significantly affect the results.

---

*This functioning of the NRAMP option is present in correction levels FIX12 and FIX14 of the code; in FIX13, only 1/NRAMP of the wire wrap effects on flow areas and wetted perimeters are included during the entire implicit initialization procedure. The full effect of the wire wrap is included at the first step taken using the explicit solution procedure regardless of the value input for NRAMP in all 3 correction levels. The important consideration relative to the current work is prevention of the full effect of the wire wrap from being present during the implicit initialization.

Steady-state calculations with COBRA-IV-I which did not use the wire wrap model did not exhibit any "drift" in the solution during a transient with time-invariant boundary conditions for either the explicit or implicit solution techniques. In these cases the channel flow areas and wetted perimeters were uniform axially but were adjusted to values reflecting a smearing of the wire wrap. The non-convergence of the COBRA-IV-I steady-state initialization procedure appears to be related to the axial variation of channel flow area and wetted perimeter introduced by the spiraling of the wire wrap around the perimeter of the fuel rods.

Cases have been run on the production version[6] of COBRA-IV-I, which is maintained on the CDC computers at Brookhaven National Laboratory by the code developers from Battelle-Pacific Northwest Laboratories, in order to investigate the various convergence problems. The results obtained on the CDC production version for all cases replicate those obtained using the single-precision IBM version at ANL. There are, thus, generic convergence problems in the COBRA-IV-I code.

In summary, there are serious convergence problems encountered when using COBRA-IV-I to model bundles of wire-wrapped pins. The results at the end of the steady-state initialization process do not appear to be correct; proper steady-state solutions must be obtained by running the code in the transient mode with constant boundary conditions and using the explicit solution technique. Additionally, for some cases the full effect of the wire wrap must be prevented from being present during the implicit initialization by using NRAMP values of 50 to 100 (depending on the magnitude of the coefficient for forced diversion flow due to spiraling of the wire wrap). These convergence problems appear to be present only when the channel flow area is variable in the axial direction (either due to an explicit geometry change or the explicit modeling of wire wrap spacers on the pins).

2. Comparison of Codes and Experiments

The benchmarking of BIFLO consists of comparisons of the code to experiments and to other computer codes (particularly those employing subchannel geometry). The task also involves comparing results obtained with the subchannel codes to the experiments to obtain confidence in the subchannel codes and to aid in translating pointwise measurements to regional averages. The work to date has used the experiments performed using Bundle 6A in the THORS facility at ORNL and the COBRA-IV-I and COMMIX-1A codes.

THORS Bundle-6A utilized 19 wire-wrapped, electrically heated fuel pin simulators in a flowing sodium environment. Results have been reported for steady-state non-boiling tests[4] and for transient tests[5] which involved boiling and dryout. Calculations have initially been focussed on the steady-state tests in order to characterize: (1) overall bundle hydraulics, (2) lateral flow effects, and (3) bundle heat losses. Application of COBRA-IV-I to these tests has been frustrated by convergence problems when the wire wrap model is used and these problems are discussed in a separate section. Some initial steady-state calculations, however, have been completed for conditions representative of THORS Bundle-6A Test-22/Run-101. The explicit solution technique was used to solve a "transient" problem with time-invariant pressure-drop boundary conditions. A properly converged steady-state solution was

obtained after 250 time steps (0.25 s). Calculations utilizing this solution procedure are continuing; adjustments to the input data are being made to reflect a better understanding of the test data. Application of BIFLO to these steady-state tests has generally given encouraging results. There is, however, a systematic difference between the calculated and measured pressure drop versus flow relationship; the source and importance of this discrepancy is being examined further. Access to a version of COMMIX-1A (Ref. 7) which is being developed in the Components Technology Division at ANL, has been obtained and the input for a 19-pin problem is being prepared. This code may be used as an alternate to the use of COBRA-IV-I code for transients which do not involve boiling due to the convergence problems encountered with COBRA-IV-I. The BIFLO benchmarking effort is planning to utilize the boiling version of COMMIX when it becomes available; the experience gained by running the non-boiling version will aid in the eventual use of the boiling version.

C. Effect of Sodium Compressibility and Steel Elasticity on Inlet Plenum Pressure Rise from Boiling in an LMFBR Loss-of-Flow Accident (Kalimullah and H. H. Hummel)

The rise of inlet plenum pressure in an LMFBR because of sodium boiling and consequent downward sodium slug ejection can have an important inhibiting effect on the velocity of such ejection, which might in turn have an important effect on an accident sequence. In the SAS code compressibility of the sodium in the inlet plenum is used to smooth pressure fluctuations in calculating the coupling of the in-core sodium flow to the sodium flow in the primary loop. It seemed to be of interest to investigate whether sodium compressibility and structural elasticity effects are of real physical importance in accident calculations.

These effects have been investigated using the one-dimensional Pressure Transient Analysis Code PTA-2,[8,9] using a single channel to model the core. The reactor model used was based on the CRBR, with the geometrical elevations and dimensions taken from the CRBR design. The free sodium surfaces in the reactor and pump vessels have been explicitly modeled. In addition to the loop-type CRBR design, a pool-type reactor has been simulated by using a pipe length between the pump outlet and the inlet plenum of 50 ft rather than 500 ft. The initial coolant flow and the bubble pressure-time history data input to the analysis were based on a SAS-3A calculation of a loss of flow accident for the CRBR reported earlier[10] (for the case assuming static sodium film on cladding, no axial expansion feedback and with clad motion).

It was found that the inlet plenum pressure buildup in the loop case was considerably larger than that in the pool case, implying an important difference in the retarding effect of the pressure buildup. This difference was caused by the difference in inertia effect of the two different liquid lengths in the inlet pipe. In either case the effect of sodium compressibility and steel elasticity on the inlet plenum pressure itself was small. For the loop case, however, the pressure difference between core and inlet plenum was relatively considerably greater when these effects were taken into account, resulting in an increase by about a factor of two in lower sodium slug ejection rate (from 1.5 ft/sec to 3.1 ft/sec). However, this ejection velocity was still small compared to that in the pool case, which was 14.3 ft/sec. Thus compressibility and elasticity effects resulted in a small reduction in the

difference in plenum pressure buildup effect between pool and loop cases. In the pool case the compressibility and elasticity effects on lower slug ejection velocity were negligible. It does not appear that these effects are large enough to require consideration in accident analysis, although it would be desirable to carry out PTA-2 calculations in which the core is modeled by two or more channels with different pressure-time curves to see if the effects are larger with such a treatment.

D. Comparison of Transient Fission Gas Release Models (H. H. Hummel and Kalimullah)

1. Gas Release Models Studied

We currently have the following transient fission gas release models available to us:

1. FRASPAR. This is an early parametric model of E. E. Gruber. It is the model used in SAS3D[11] and has also been incorporated into SAS/EPIC.

2. FRAS3.[12] This is the current version of the FRAS series of codes under development for some years by E. E. Gruber in the RAS Division of ANL.

3. NEFIG.[13,14] This is the fission-gas release model currently used in the UK fuel pin modeling code FRUMP. This code and FRAS3 have been made available to us in a form that facilitates comparison of these codes through the courtesy of E. E. Gruber.

4. GRASS-SST.[15] This code has been developed by J. Rest of the MSD Division of ANL as part of the NRC RSR LWR safety program.

5. FASTGRASS.[16] This is a fast running version of GRASS-SST and is still under development. It has been made available to us through the courtesy of J. Rest.

FRASPAR does not actually model the release of fission gas but is a parametric fit to an early version of FRAS. The release rate is adjustable through an input parameter GRAINM. This code executes rapidly enough to be used in a SAS-type calculation, but is useful only to the extent that it can adequately reproduce experiment or the results of more exact calculations.

2. Comparison of Models

In all cases the major mechanism for release of fission gas from a fuel grain is assumed to be biased migration of gas bubbles under influence of a temperature gradient. Random migration can also make a contribution for small bubbles, but will be ignored in the present discussion. None of the codes are applicable once fuel melting starts. For FRAS3 and NEFIG bubble migration is assumed to be by surface diffusion, a process in which fuel lattice atoms jump on the surface of a gas bubble. If a temperature gradient is present the lattice atoms will jump preferentially from the hot toward the

cold side of the bubble, causing the bubble to move up the temperature gradient. For biased migration the bubble velocity v_B in NEFIG, GRASS-SST and FASTGRASS is proportional to

$$\frac{D_s \nabla T}{R_B T^2},$$

where D_s is the surface diffusion coefficient, R_B is the bubble radius, T is fuel temperature at the bubble, and ∇T is the thermal gradient at the bubble surface. The same relation is used in FRAS3, except that for small bubbles a correction is made to account for the fact that the lattice atom jump distance is greater than the bubble diameter.[17] This correction is not important for the cases considered here.

The surface diffusion coefficient used in FRAS and NEFIG has the same temperature dependence, but the pre-exponential factor used in FRAS is 1.75 times that assumed for NEFIG. In GRASS-SST and FASTGRASS surface diffusion is assumed to provide an upper limit for bubble velocity which applies for bubbles far below equilibrium size (for which there is equilibrium between gas pressure and fuel surface tension, neglecting any fuel hydrostatic pressure). The condition of being far from equilibrium is expressed through a variable α[15] (BETAB in the code) which then has a value of 1.0, while at equilibrium α=0.0. If α=1.0, so that surface diffusion is assumed in GRASS-SST and FASTGRASS, the value of the surface diffusion coefficient assumed in these codes ranges from 0.87 times the one used in NEFIG at fuel melting temperature down to 0.15 times the NEFIG value at 1900°C. If α<1 the surface diffusion coefficient in GRASS-SST or FASTGRASS is replaced by a coefficient dependent on the value of α and having an even lower value. However, α was found to have the value 1.0 most of the time in the cases studied here.

In both FRAS and NEFIG the ∇T term is set equal to a factor β=1.5 times the mean temperature gradient in the fuel. This factor, which accounts for the perturbing effect of the low thermal conductivity of the bubble on fuel temperatures in the vicinity of the bubbles,[18] is not used in GRASS-SST and FASTGRASS, as its applicability for these codes is considered questionable.[19]

Another factor affecting gas release rate in biased migration is bubble size, because of the inverse dependence of bubble velocity on bubble size. In NEFIG and in FASTGRASS in order to obtain a fast-running code only a single bubble size class is considered, with this size varying during the transient. In FRAS3 and GRASS-SST a number of bubble size classes are considered. The mean bubble size increases during a transient because of bubble coalescence so that the relative populations of the larger size classes increase during a transient. The time variation of the single bubble size in NEFIG corresponds fairly well to the variation of the average bubble size in FRAS3. In NEFIG the supply of lattice vacancies necessary to allow bubbles to grow to equilibrium size is limited by requiring these vacancies to diffuse from grain boundaries. No such limitation is imposed in FRAS3, so that the mean bubble size tends to be larger. However, the resultant reduction in bubble velocity is about compensated by the assumption of a larger surface diffusion coefficient. The bubble sizes in GRASS-SST and FASTGRASS tend to be smaller than

those in FRAS3 and NEFIG, which acts to offset the lower diffusion coefficient assumed.

Having determined the bubble velocity as a function of time, it is necessary to specify how the gas release from a fuel grain is related to a given biased bubble migration as a function of time. If a reduced bubble migration distance x is defined as

$$x = \frac{\text{migration distance}}{\text{grain diameter}},$$

in GRASS-SST and FASTGRASS the fractional gas release f_G from a grain as a function of time is assumed to be

$$f_G = 2.37x.$$

In NEFIG and FRAS3 a model is employed in which two initially coincident spheres, one representing the gas and the other the fuel grain, are assumed to move apart as the bubbles migrate.[17] This model leads to an expression for fractional gas release

$$f_F = \frac{3}{2}x - \frac{1}{2}x^3$$

which reduces to $f_F = \frac{3}{2}x$ for small x.

At $x = 0.42$, $f_G = 1.00$, while $f_F = 0.593$. Thus f_G/f_F ranges from 1.58 at small x to 1.67 at $x = 0.42$. This nearly balances the omission of the factor β in GRASS-SST and FASTGRASS.

With the gas released from within the grain, it can still be held up on grain boundaries or grain edges (intersections of grain boundaries). Such holdup is not currently modeled in NEFIG. In FRAS3 grain boundary effects are modeled; they reduce gas release as a function of time by about 2% of the original gas content, not a large effect. In GRASS-SST and FASTGRASS both grain boundary and grain edge holdup are modeled. This was found to have a considerable effect on gas release as is discussed below.

3. Cases Studied

Results from applying these codes to two transients are given here. One of these transients is the HEDL FGR-39 experiment.[20] This was an out-of-pile experiment in which irradiated fuel was heated at a rate of ~200°C/sec with a temperature gradient in the range 3000-5000°C/cm. Grain diameter was taken as 38μm. Analysis of this experiment with NEFIG is discussed in Reference 14. In there it is stated that the authors calculated larger temperature gradients for this experiment than those reported by HEDL, which also had to depend on calculations, the differences arising from different fuel thermal conductivities resulting from assumed radially varying fuel oxygen-to-metal ratio. Agreement with experiment was felt to be satisfactory with these larger temperature gradients. In our calculations, shown in Fig. 1, we have used the temperature data originally supplied by HEDL. The calculated fractional release given by

FRAS and NEFIG as a function of fuel temperature using these temperature data is well below the experimental curve. FRAS and NEFIG give practically identical results. There is a small discrepancy in release from the fuel grains in that there is about 2% fission gas holdup on grain boundaries in FRAS. This effect is not modeled in NEFIG. GRASS-SST gives lower values because of the lower diffusion coefficient used, in spite of a somewhat smaller average bubble size. The release from the fuel is enhanced by 4.8% of the original gas from grain boundaries and edges during the transient. FRASPAR with GRAINM=0.1 is reasonably close to experiment but larger than FRAS or NEFIG. With GRAINM=0.4, used a number of times in the past, the calculated release is much larger than with FRAS or NEFIG.

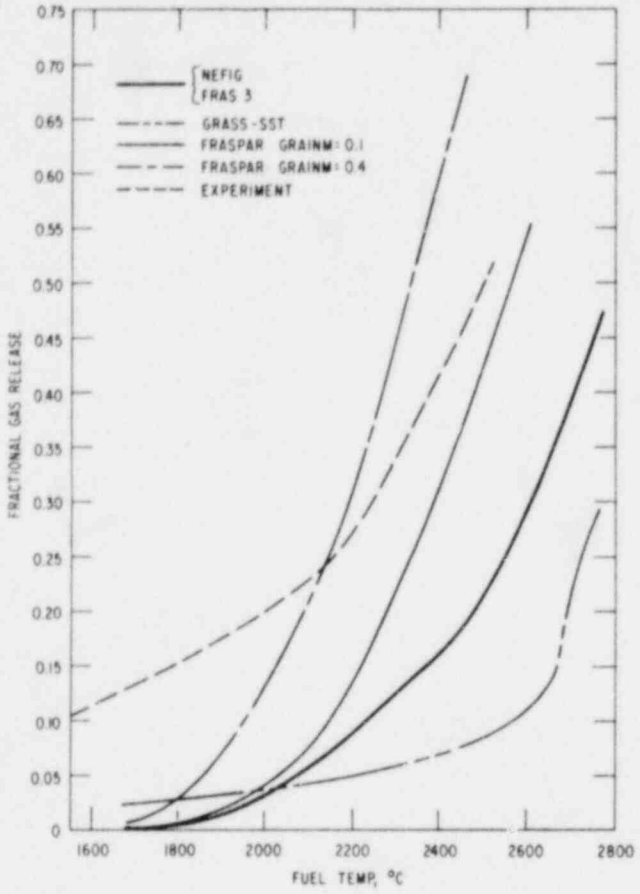

Fig. 1.

Comparison of calculation methods and experiments for fission gas releases in HEDL experiment FGR-39.

The other transient for which calculations were made is a more rapid one corresponding to what might be expected in a LOF-TOP situation. The time-temperature curve is the same as that designated as "Curve 2" in Reference 21. The heating rate for this transient during most of the gas release is in the range 4000-5000°C/sec. The temperature gradient was assumed to be 10,000°C/cm, and the fuel grain size to be 17μm. Because of the faster heating rate, the gas release for a given fuel temperature, shown in Fig. 2, is seen to be well below that for the FGR-39 experiment in spite of the smaller grain size and larger temperature gradient assumed in this case. The initial gas concentration assumed in this case, 2.0×10^{20} atoms/cm^3, was slightly larger than the 1.6×10^{20} assumed for FGR-39, which would reduce the gas release slightly. FRAS3 gives slightly lower results than NEFIG in this case. A large part of this difference corresponds to holdup of gas on grain boundaries in FRAS3. In this case FRASPAR with GRAINM=0.1 gives results below those from FRAS3 and NEFIG; with GRAINM=0.2 agreement is fairly close. With GRAINM=0.4 the results are again well above those of the other codes. The implication from the results with these two transients is that the most suitable value for GRAINM shifts from one transient to another. This suggests that the parametric model may be of rather limited usefulness unless it turns out to be possible to establish satisfactory rules for selecting GRAINM in any particular situation.

GRASS-SST and FASTGRASS give results that differ from those of FRAS3 and NEFIG because of differing parameter and modeling assumptions relating to surface diffusion coefficient, average bubble size, and holdup of fission gas on grain boundaries and edges. Gas release tends to be lower than that from FRAS3 and NEFIG.

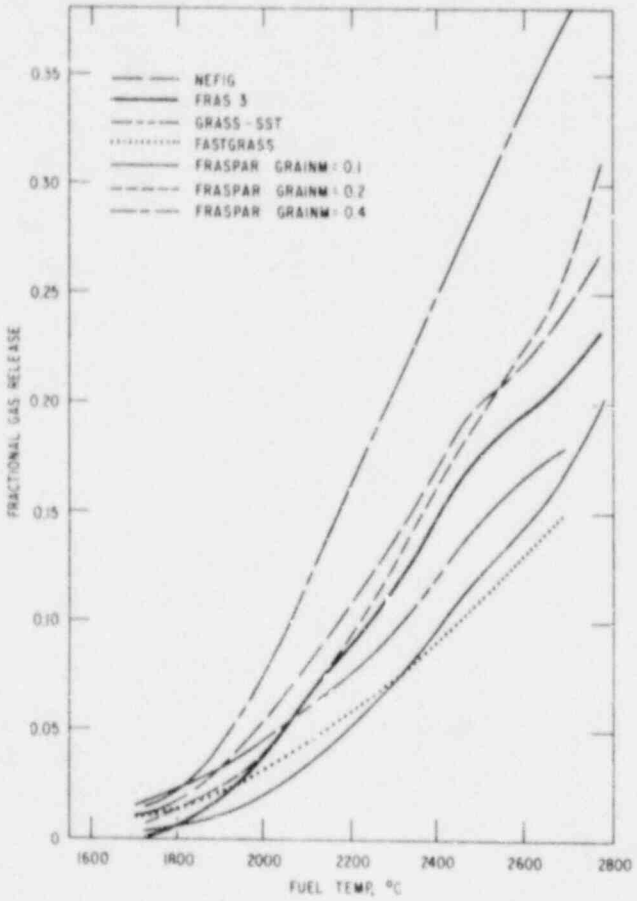

Fig. 2.

Comparison of fission gas release calculation methods for heating rate of 4000-5000°C/sec, temperature gradient 10,000°C/cm, fuel grain diameter 17 μm, initial gas concentration 2.0×10^{20} atoms/cm^3.

Although the results from GRASS-SST and FASTGRASS are relatively close to each other, there were compensating effects in this case between release from the grains themselves and from grain boundaries and edges, for which the two codes gave considerably different results. Release from the grains with GRASS-SST was comparable to that from NEFIG and FRAS3 because a small average bubble size more than offset the lower diffusion coefficient, but there was large holdup on grain boundaries and edges. The bubble size in FASTGRASS was considerably larger. As remarked above, the modeling in FASTGRASS is still under development.

4. Conclusions

FRAS3 and NEFIG give similar results for widely varying heating rates. The most suitable value for the GRAINM parameter in FRASPAR seems to depend on the particular transient under consideration.

II. THREE-DIMENSIONAL CODE DEVELOPMENT FOR CORE THERMAL-HYDRAULIC ANALYSIS OF LMFBR ACCIDENTS UNDER NATURAL CONVECTION CONDITIONS

(A2018)

A. Introduction

The objective of this program is to develop computer programs (COMMIX and BODYFIT) which can be used for either single-phase or two-phase thermal-hydraulic analysis of reactor components under normal and off-normal operating conditions. The governing equations of conservation of mass, momentum, and energy are solved as a boundary value problem in space and initial value problem in time.

COMMIX is a three-dimensional, transient, compressible flow computer code for reactor thermal-hydraulic analysis. It is a component code and uses a porous medium formulation. The concept of volume porosity, surface permeability, and distributed resistance and heat source (or sink) is employed in the COMMIX code for quasi-continuum (or rod-bundle) thermal-hydraulic analysis. It provides a greater range of applicability and an improved accuracy than subchannel analysis. By setting volume porosity and surface permeability equal to unity, and resistance equal to zero, the COMMIX code can equally handle continuum problems (reactor inlet or outlet plenum, etc.).

BODYFIT is a three-dimensional, transient, compressible flow computer code for reactor rod bundle thermal-hydraulic analysis. This is also a component code, and it uses a boundary-fitted coordinate transformation. The complex rod bundle geometry is transformed into either rectangular or cylindrical coordinates with uniform mesh. Thus, the physical boundaries, including each rod, coincide with computational grids. This allows the Navier-Stokes equations, together with the boundary conditions, to be represented accurately in the finite-difference formulation. Thus, the region in the immediate vicinity of solid surfaces, which is generally dominant in determining the character of the flow, can be accurately resolved.

B. COMMIX-1A, Single Phase Code Development (H. M. Domanus, M. J. Chen and W. T. Sha)

1. Computational Techniques

In an effort to speed the COMMIX-1A calculation of transients when the flow is reduced to a natural circulation condition, an implicit energy option has been developed and implemented into COMMIX-1A.

The user has the option of selecting either the explicit or implicit formulation. In addition, if the implicit formulation is selected, the user can specify the solution technique as either a cell-by-cell Jacobi type solution technique, or a cell-by-cell successive over-relaxation (SOR) iterative technique. Implicit coupling of the thermal structures and the duct walls was found to be necessary in the implicit formulation of the energy equation.

Using the new implicit energy option, the natural circulation transient simulation of the Sodium Loop Safety Facility (SLSF) P2 test was done. Because

the solution sequence utilizing the implicit energy option permits a larger time step size, preliminary indications are that the simulation can be done in one-fourth the computer time required last summer when the explicit energy formulation was used.

The cylindrical coordinate option of COMMIX-1A was re-examined. Particular emphasis was placed on flow directly through the origin in the r-θ plane. It was found that no special treatment of the mass, momentum or energy equations is required in the vicinity of the origin. The cell integrated formulations of the mass, momentum and energy equations used in COMMIX-1A adequately model the thermohydrualic behavior even when there is flow through the origin.

2. Horizontal Pipe Transient

The results of the simulation of a thermal-hydraulic transient in a pipe using the COMMIX-1A code are presented. The purpose of the simulation was to investigate the thermal buoyancy effects on temperature and velocity distributions in a pipe. Analyses of thermal buoyancy induced flows in piping are very important in both steady-state and transient operating conditions; the buoyancy force greatly alters hydraulic resistance and creates large, local temperature gradients.

The pipe analyzed was horizontal and 21.336 m (70 ft) long. The inner diameter was 0.4318 m. The pipe wall thickness was 0.0127 m and is made of SS 316. Since the thermal-hydraulic conditions are symmetric with respect to the vertical center line, one needs to consider only half of the circular geometry.

As shown in Fig. 3, the 21.336 m pipe was partitioned into thirty-five equal 0.6096 m lengths. The radial direction was partitioned into five 0.08636 m equal lengths. The azimuthal direction was partitioned into six equal 30° angles.

The following assumptions were employed in this simulation:

i) The shape of the inlet velocity distribution is parabolic throughout the whole transient.

ii) The temperature of the incoming sodium is uniform over the inlet cross section.

iii) Turbulent eddy transport of energy and momentum is constant throughout the whole transient.

iv) Pipe inner surface is non-adiabatic and outer surface is adiabatic.

Figures 4 and 5 show the flow and temperature transient at the inlet.

Figures 6-8 show transient liquid sodium temperatures at various axial and radial locations of the pipe.

Because of the parabolic inlet velocity distribution and the temperature decrease at the inlet, cooler sodium penetrates into the central portion of the pipe. This causes, earlier in the transient, cooler temperatures in the upper central region and warmer temperatures in the bottom annular region. As a result of further flow redistribution, considerable stratification (top to bottom temperature difference in excess of 65°C) was observed in the later part of the transient.

Figures 9-12 show isothermal lines in the vertical cross-section through the centerline at various times. We can see in these figures that the temperature near the wall is higher than the temperature at the center of the pipe. This is due to thermal interaction between pipe wall and liquid sodium. As the transient proceeds, the temperature falls to a minimum of about 220°C by 80 seconds, then increases to 290°C by the end of the 200 second transient. By 100 seconds, as shown in Fig. 10, this drop and subsequent rise causes a cold spot to be entrained in the pipe. From Figs. 11-12, we can see that, as time proceeds, the cold spot is being convected and diffused down the pipe and finally out the exit.

C. COMMIX-2, Two-Phase Code Development (J. G. Bartizis, J. L. Krazinski, C. C. Miao, V. L. Shah and W. T. Sha)

Two alternate solution procedures for COMMIX-2 are under development. Progress in each procedure is summarized below.

1. Line-by-Line Solution Procedure

Development of the COMMIX-2 (two-phase) computer code continued during the previous quarter. Two problems were run to test the two-fluid model. The first case was a phase separation problem in which gravity caused a uniform vapor/liquid mixutre to separate into regions of pure liquid and pure vapor. The running time obtained with the current line-by-line technique was 3-4 times faster than the running time with the previous cell-by-cell approach.

The second problem studied was 2-D flow in a heated duct. Subcooled liquid sodium enters the duct and begins to boil as it passes through the heated duct. The Nigmatulin boiling model[22] was used for computing evaporation rate. Some preliminary results were obtained for this problem, although further work is necessary to improve the numerical efficiency and accuracy.

An option has been incorporated in the COMMIX-2 code to permit running of single-phase, gas-flow problems. This option allowed further testing of the vapor-phase section of the code. Additional options for running one-dimensional and two-dimensional problems were also implemented in the code. These capabilities allow solution of 1-D, 2-D, and 3-D single-phase (liquid or vapor) and two-Phase flow problems.

2. Analytic Rebalance Technique

In regard to the development of Analytic Rebalance Technique (ART),[23] the efforts were devoted to obtain solution of a phase separation problem. For this first test problem, at $t = 0$, we have an isothermal uniform mixture of

vapor and liquid in a recangular vertical closed duct. As time proceeds, due to gravity, vapor starts to move up and liquid starts to move down. Figure 13 shows the void fraction distribution along the duct at various time steps. Figure 14 shows the upper and lower bound of total mass residue with time. The computation is carried out with the value of interfacial drag coefficient $K = 10^3 kg/m^3 s$. Complete separation of liquid and vapor is observed at $t = 400$ ms. The calculation required less than 10 seconds of computer time on the IBM-195. This is a significant improvement in the computational time in comparison to the computational time required by the previous cell-by-cell approach. NRC standard problem No. 1 is now selected as a second test problem for ART approach.

D. BODYFIT-1, Single-Phase Code Development (B. C-J. Chen and W. T. Sha)

In the area of BODYFIT development for 3-D geometry, the coding of the 3-D transformed Navier-Stokes equations has been completed. A simple test case of a distorted pin inside a hexagonal duct wall was set up for the purpose of debudgging. The geometric configuration of the test problem is given in Figs. 15 through 19. Twelve axial levels and 360 radial cells were used for this problem. The radial coordinate lines for axial levels 1, 7, and 12 are shown in Figs. 15, 16, and 17 respectively. The axial coordinate lines along sections AA and BB or Fig. 15 are shown in Figs. 18 and 19, respectively. The axial velocity plots are presented in Figs. 20 and 21. We can see from these plots that velocity profiles have qualitatively correct shapes.

The energy equation has also been programmed into the code. A sample case has been performed. Figure 22 shows the temperature distribution along section AA, and Fig. 23 shows the temperature distribution along section BB. The inlet temperature has been subtracted from the temperature plots in Figs. 22 and 23. All the profiles appear to be correct.

The efforts were also devoted to carry out parametric studies for 3-D distorted geometry. For the cases that were investigated, the optimum values of relaxation factors were found to be 0.7 for both the velocity and temperature calculations. Although we have not done an exhaustive parametric study, the results that we have obtained so far, provide us a good base for further investigation.

Also we have completed programming of one equation (k) and two equations (k, ε) turbulence models for two dimensional cases. We are now testing these two models for 7-pin hexagonal geometry. Preliminary calculations show that the turbulence viscosities are in the order of 50 to 150 times greater than the laminar viscosities. This ratio is greater near the solid wall than that at the middle of the flow region. This observation is consistent with the past experience we have had on the application of the two equations turbulence model.

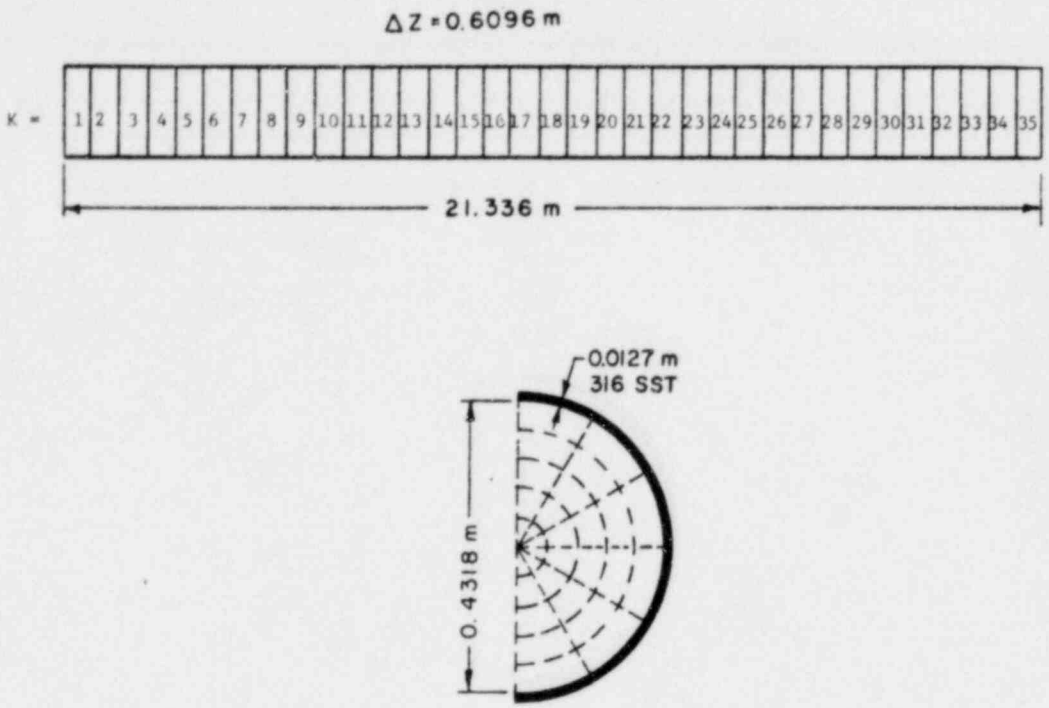

Fig. 3. Axial, Radial, and Azimuthal Partitioning used for Pi Simulation.

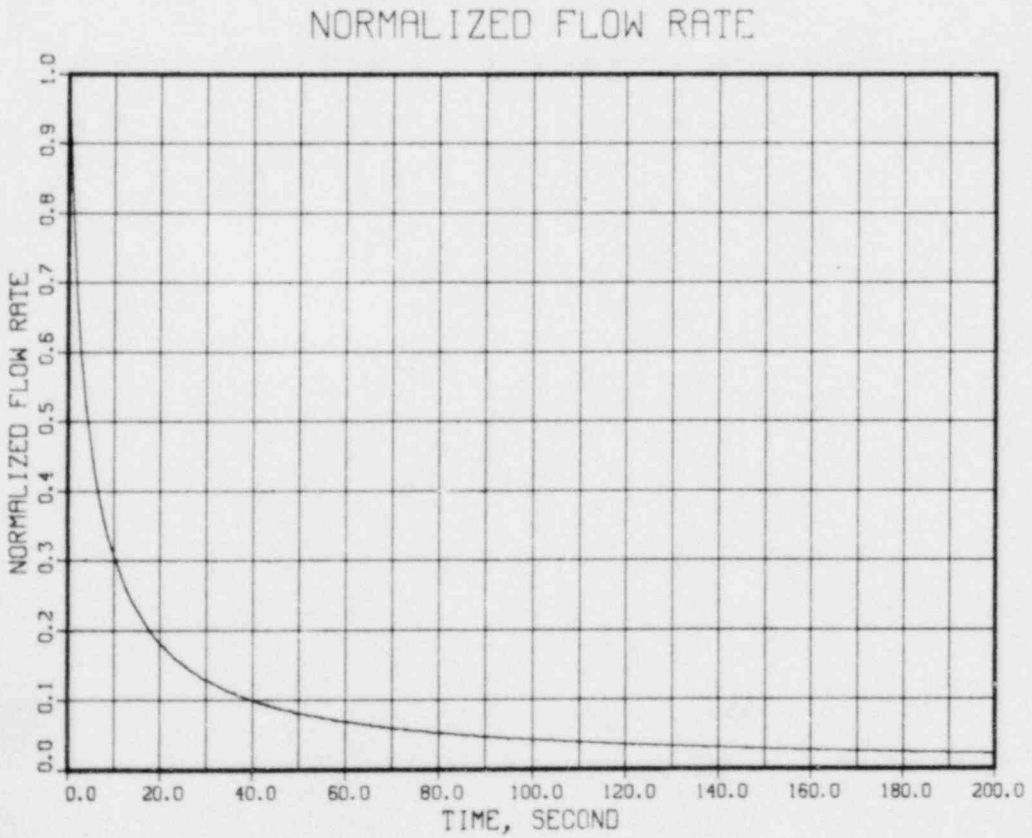

Fig. 4. Normalized Inlet Velocity Transient.

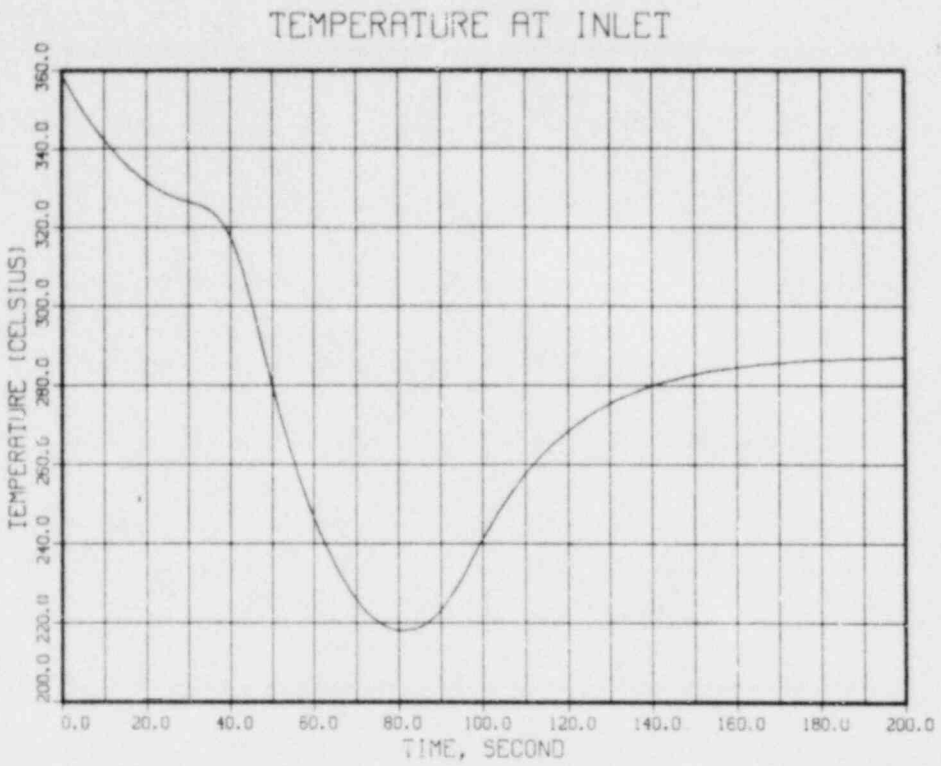

Fig. 5. Inlet Temperature Transient.

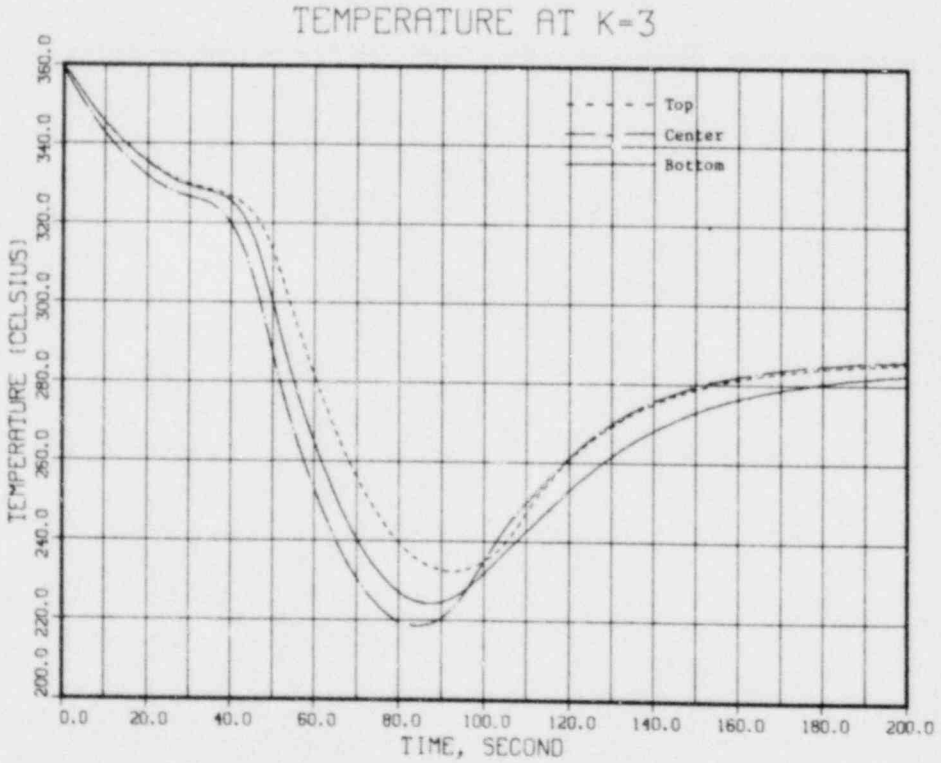

Fig. 6. Transient Temperature at K = 3, Z = 1.524 m.

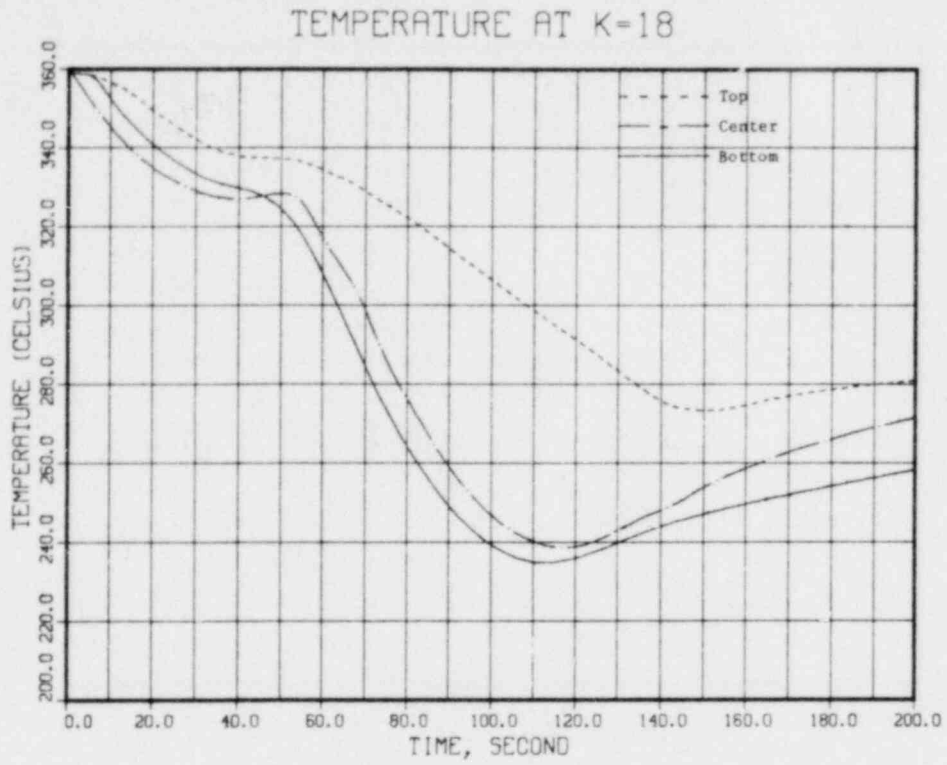

Fig. 7. Transient Temperature at K = 18, Z = 10.668 m.

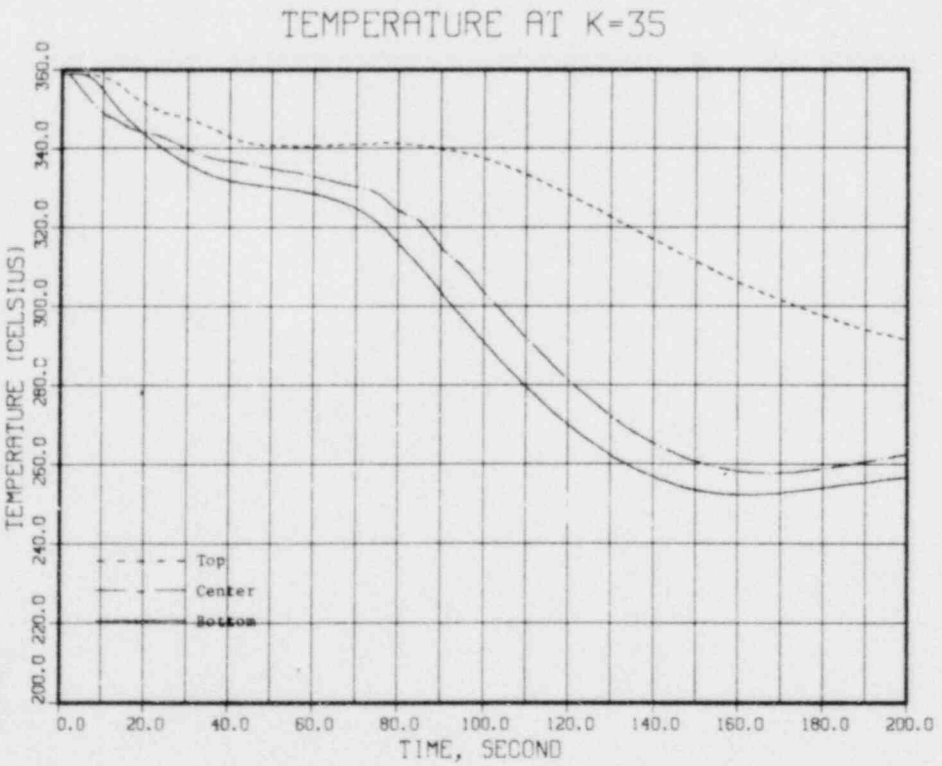

Fig. 8. Transient Temperature at K = 35, Z = 21.0312 m.

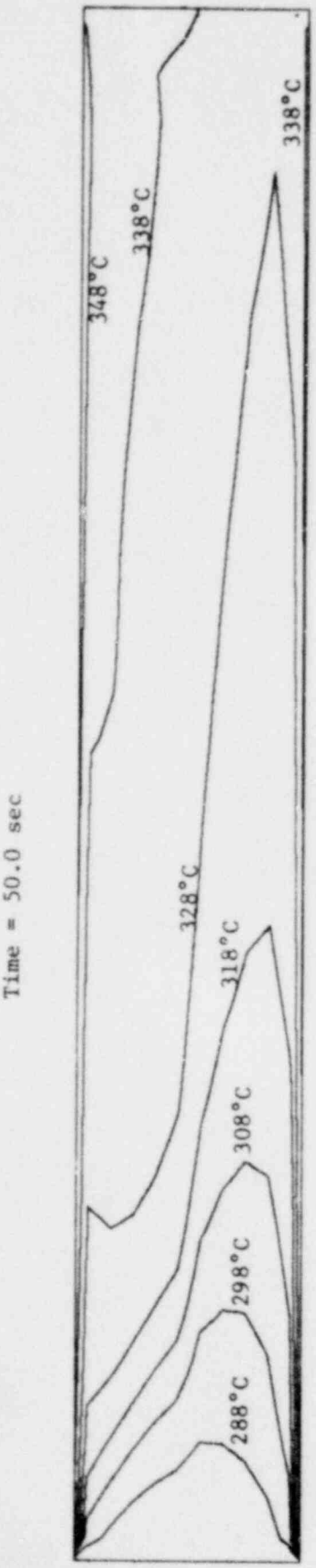

Fig. 9. Temperature Distribution of Vertical Cross Section through Centerline at t = 50.0 sec.

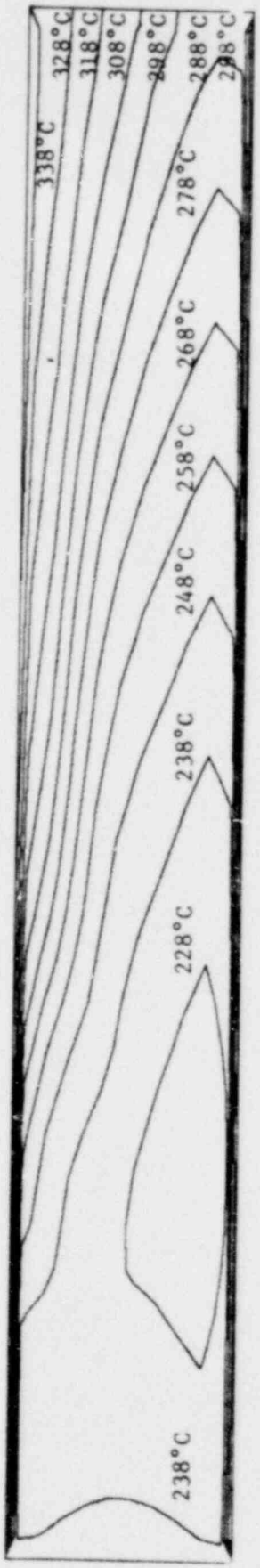

Fig. 10. Tempeature Distribution of Vertical Cross Section through Centerline at t = 100.0 sec.

Time = 150.0 sec

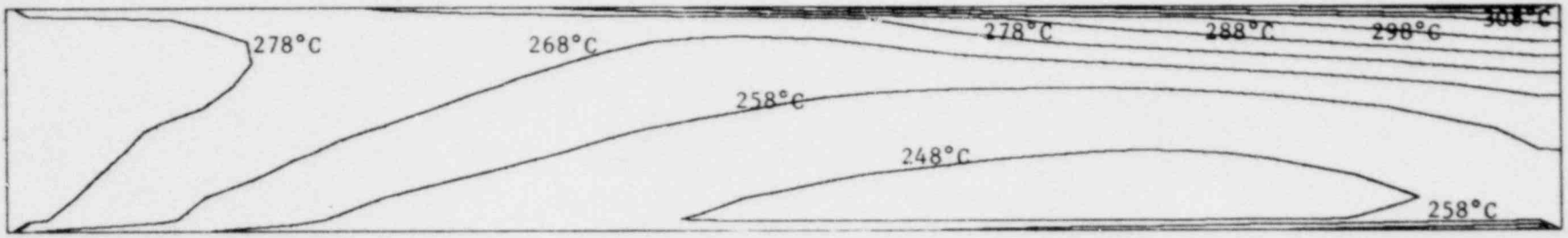

Fig. 11. Temperature Distribution of Vertical Cross Section through Centerline at t = 150.0 sec.

Time = 200.0 sec

Fig. 12. Temperature Distribution of Vertical Cross Section through Centerline at t = 200.0 sec.

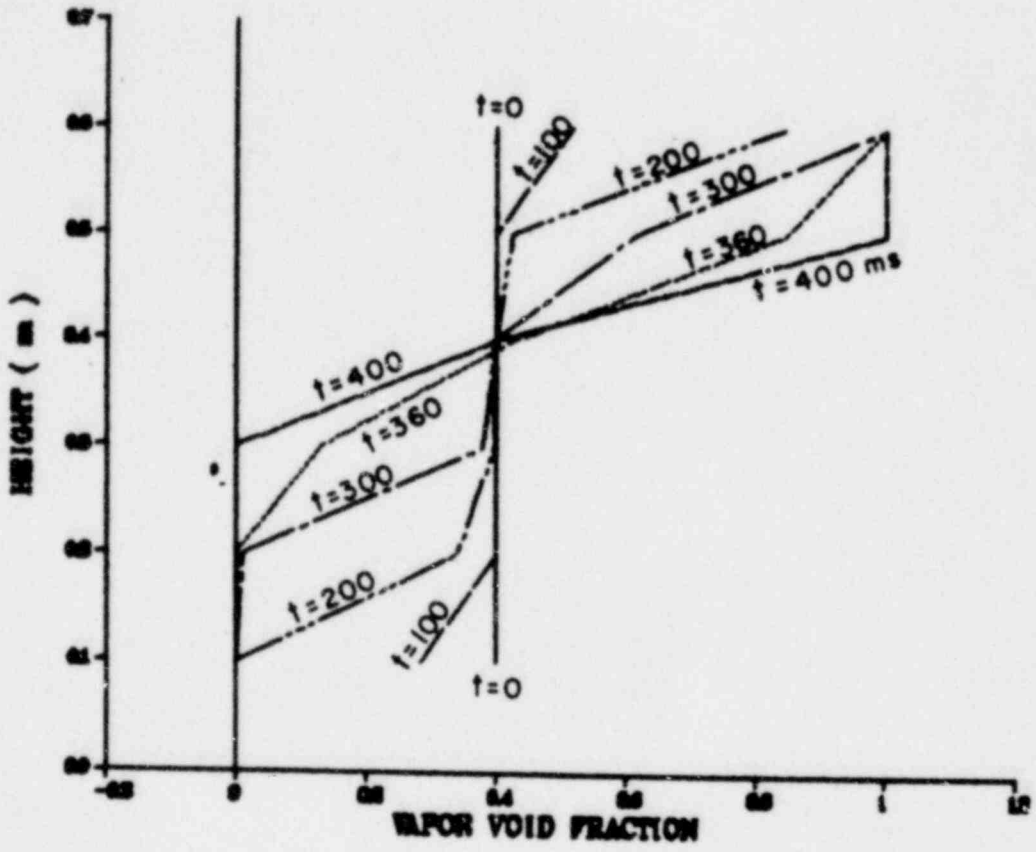

Fig. 13. Variations of Void Fraction with Time.

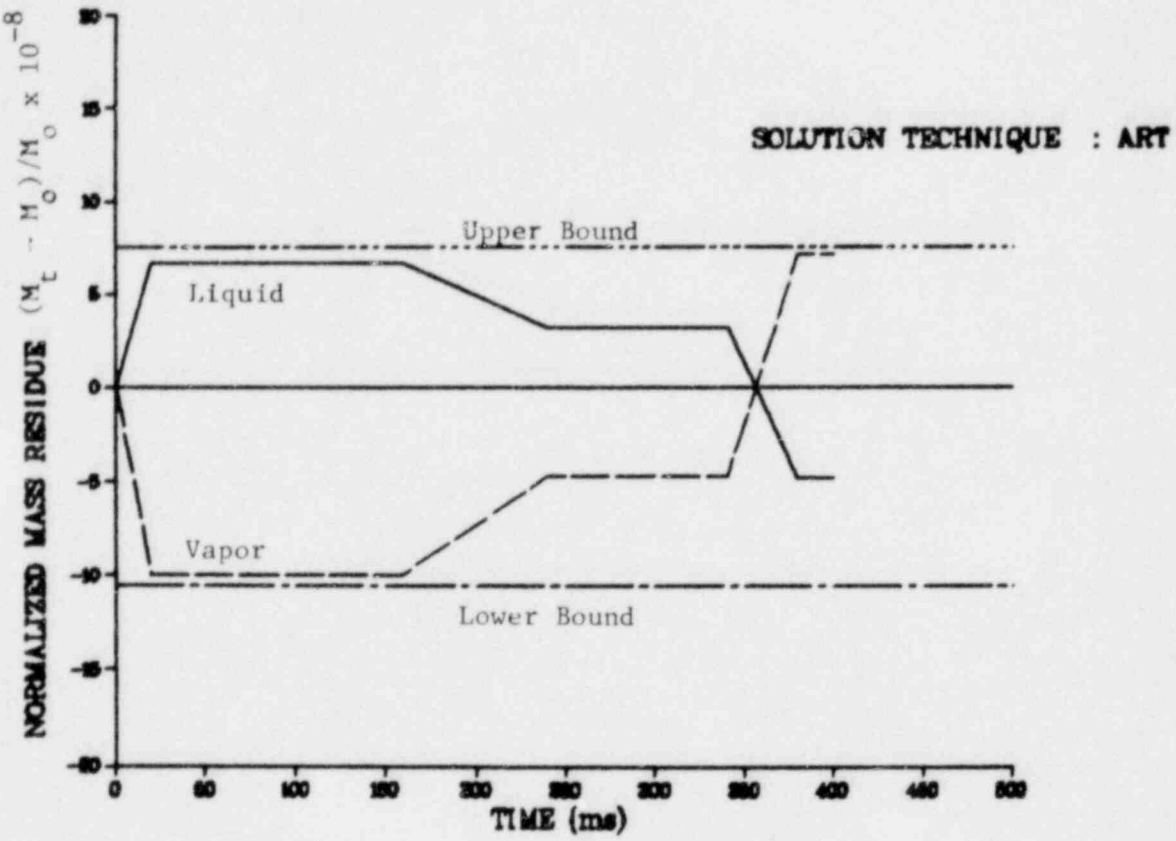

Fig. 14. Mass Residue Analysis

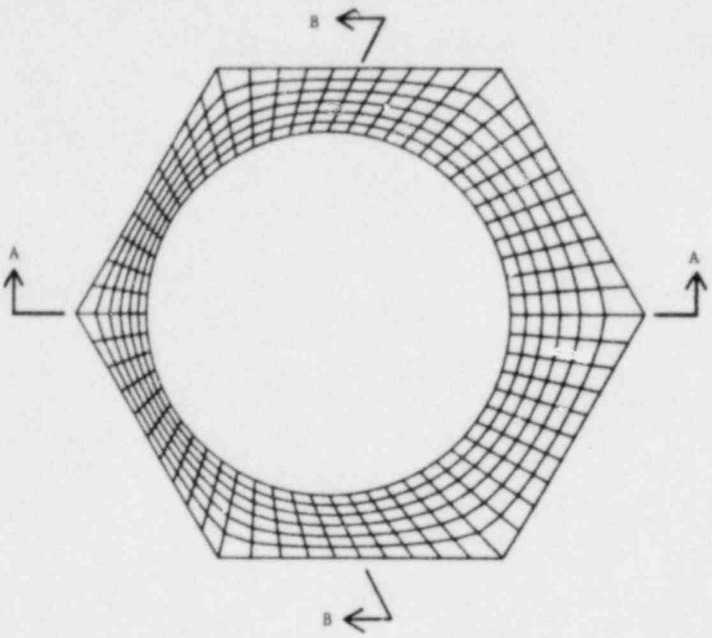

Fig. 15.
Radial Coordinate Lines for Level 1.

Fig. 16.
Radial Coordinate Lines for Level 7.

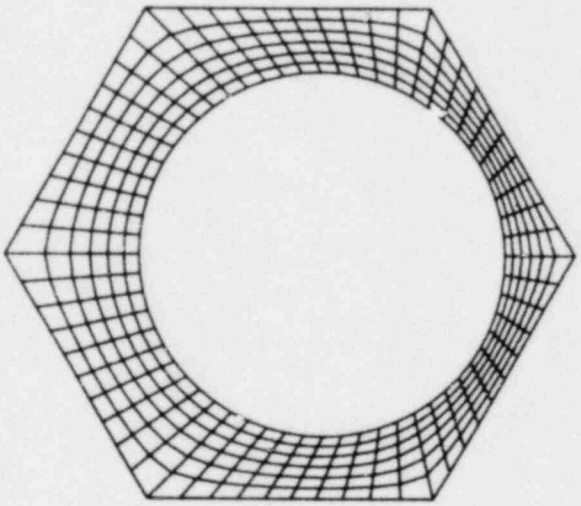

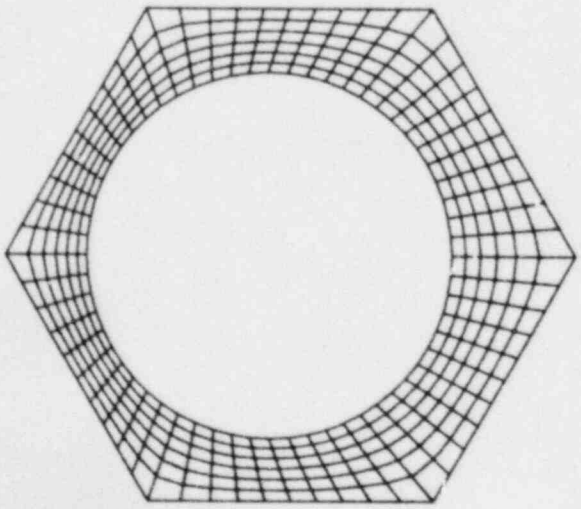

Fig. 17.
Radial Coordinate Lines for Level 12.

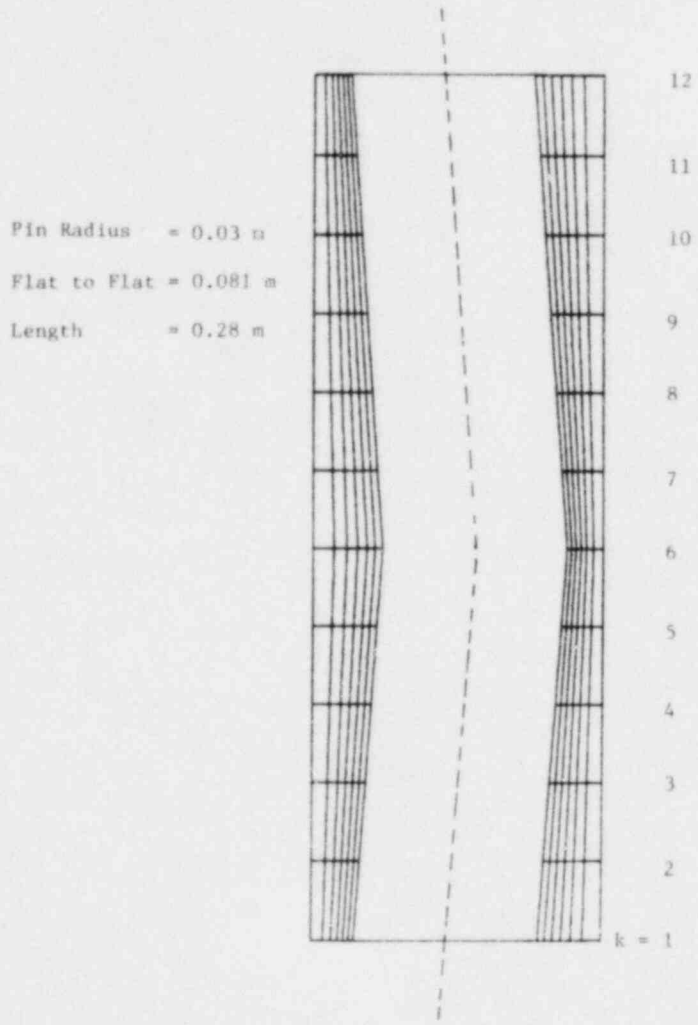

Fig. 18.
Computational Cells Along Section AA.

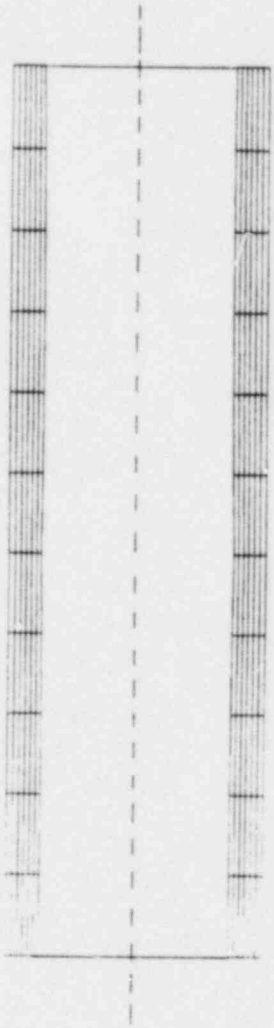

Fig. 19.
Computational Cells Along Section BB.

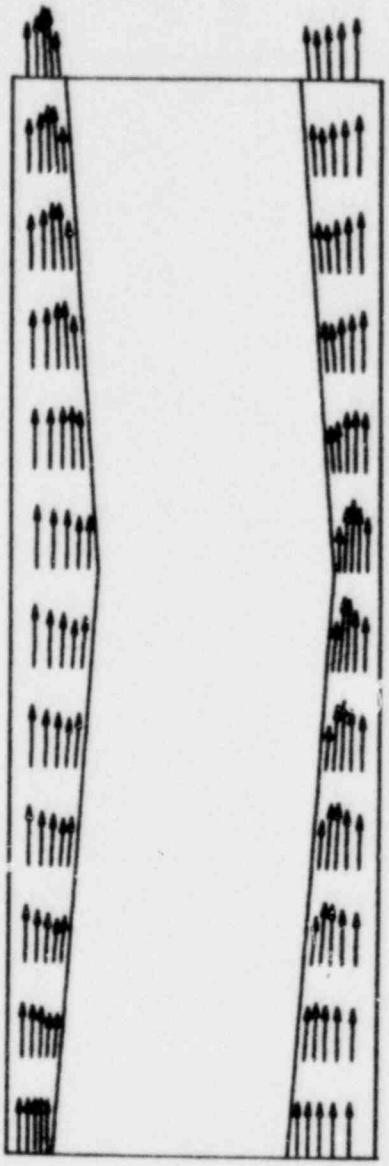

Fig. 20.

Axial Velocity Profile
along Section AA
of Figure 15.

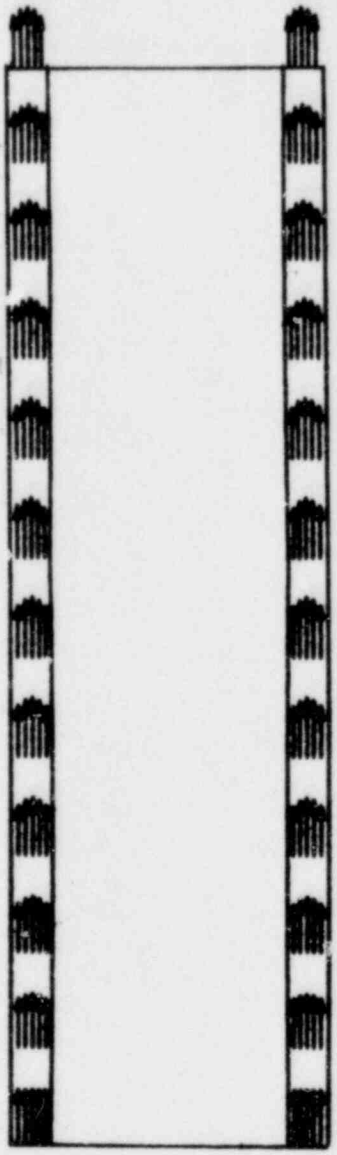

Fig. 21.

Axial Velocity Profile
along Section BB
of Figure 15.

Axial Velocity = 0.01 m/s

Flow Rate = 0.0238 kg/s

Power = 0.431×10^3 watt

Heat Flux = 10^4 watt/m^2

ΔT = 14.5°C

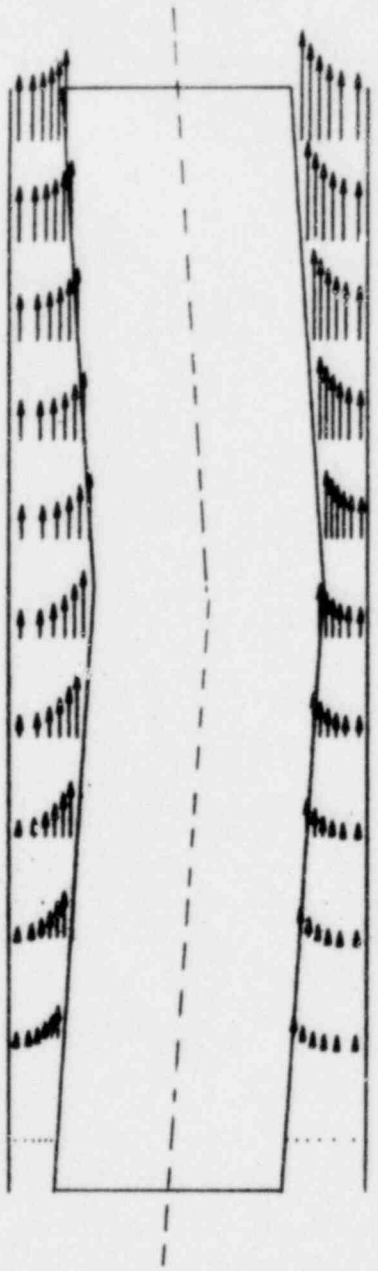

Fig. 22. Axial Temperature Plot Along Section AA.

Axial Velocity = 0.01 m/s

Flow Rate = 0.0238 kg/s

Power = 0.431×10^3 watt

Heat Flux = 10^4 watt/m^2

ΔT = 14.5°C

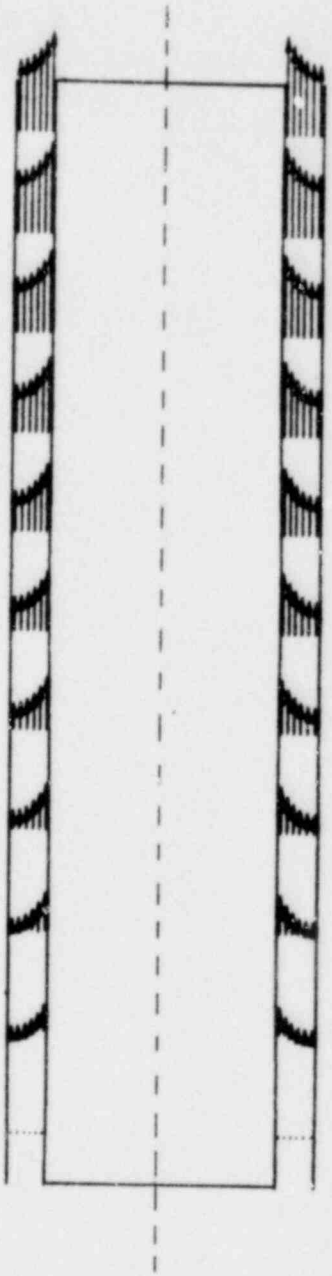

Fig. 23. Axial Temperature Plot Along Section BB.

REFERENCES

1. J. J. Sienicki and P. B. Abramson, *The TWOPOOL Strategy and the Combined Compressible/Incompressible Flow Problem,* Proc. of the Topical Meeting on Computational Methods in Nuclear Engineering, Williamsburg, Virginia, April 23-25, 1979, Vol. 1, p. 68, Amer. Nucl. Soc. (1979).

2. J. J. Sienicki, Physics of Reactor Safety Quarterly Report, October-December 1979, ANL-80-25, p. 5, Argonne National Laboratory (March 1980).

3. C. L. Wheeler et al., *COBRA-IV-I: An Interim Version of COBRA for Thermal-Hydraulic Analysis of Rod Bundle Nuclear Fuel Elements and Core,* BNWL-1962, Battelle-Pacific Northwest Laboratories, Richland, WA (March 1976).

4. J. L. Wantland et al., *Steady-State Sodium Tests in a 19-Pin Full-Length Simulated LMFBR Fuel Assembly - Record of Steady-State Experimental Data for THORS Bundle 6A,* ORNL/TM-6106, Oak Ridge National Laboratory, Oak Ridge, TN (March 1978).

5. R. J. Ribando et al., *Sodium Boiling in a Full-Length 19-Pin Simulated Fuel Assembly (THORS Bundle 6A),* ORNL/TM-6553, Oak Ridge National Laboratory, Oak Ridge, TN (January 1979).

6. C. W. Stewart, personal communication, Battelle-Pacific Northwest Laboratories (January 24, 1980).

7. W. T. Sha et al., *COMMIX-1: A Three-Dimensional Transient Single-Phase Component Computer Program for Thermal-Hydraulic Analysis,* ANL-77-96, Argonne National Laboratory, Argonne, IL (September 1978) and H. M. Domanus and R. C. Schmitt, personal communication, Argonne National Laboratory (February 20, 1980).

8. C. K. Youngdahl and C. A. Kot, *PTA-1, A Computer Program for Analysis of Pressure Transients in Hydraulic Networks, Including the Effects of Pipe Plasticity,* ANL-76-64, Argonne National Laboratory, Argonne (November 1976).

9. Y. W. Shin and W. L. Chen, *Numerical Fluid-Hammer Analysis by the Method of Characteristics in Complex Piping Networks,* Nucl. Eng. Des., 33, pp. 357-369 (1976).

10. H. H. Hummel, P. A. Pizzica and Kalimullah, *Studies of Unprotected Loss-of-Flow Accidents for the Clinch River Breeder Reactor,* ANL-76-51, Argonne National Laboratory, Argonne, IL (April 1976).

11. W. R. Bohl et al., *An Analysis of the Unprotected Loss-of-Flow Accident in the Clinch River Breeder Reactor with an End-of-Equilibrium Cycle Core,*" ANL/RAS 77-15, Argonne National Laboratory (May 1977).

12. E. E. Gruber and E. H. Randklev, *Comparions of Fission-Gas Effects in a Transient Overpower Test (HUT 5-7A) to FRAS3 Code Prediction,* Proc. of the International meeting on Fast Reactor Safety Technology, Seattle, Washington, p. 2050 (August 19-23, 1979).

13. J. R. Matthews and M. H. Wood, *Modeling the Transient Behavior of Fission Gas*, J. Nucl. Material, 84, pp. 125-136 (1979).

14. M. H. Wood, J. R. Matthews and H. R. Matthews, *Comparison of Experiment and NEFIG Model Calculations of Transient Fission Gas Behavior*, J. Nucl. Material, 87, pp. 167-174 (1979).

15. J. Rest, *GRASS-SST: A Comprehensive Mechanistic Model for the Prediction of Fission-Gas Behavior in UO2-base Fuels during Steady-State and Transient Conditions*, NUREG/CR-0202 (ANL-78-53), Argonne National Laboratory, Argonne, IL (June 1978).

16. J. Rest, *Light Water Reactor Safety Research Program: Quarterly Progress Report*, October-December 1978, NUREG/CR-0828 (ANL-79-18) p. 20, Argonne National Laboratory, Argonne, IL.

17. E. E. Gruber, *A Generalized Parametric Model for Transient Gas Release and Swelling in Oxide Fuels*, ANL-77-2, Argonne National Laboratory, Argonne, IL (January, 1977).

18. H. S. Carslaw and J. C. Jaeger, *Conduction of Heat in Solids*, Second Ed. p. 426, Oxford University Press, Inc., New York (1959).

19. J. Rest, Private Communication (1980).

20. C. A. Hinman and O. D. Slagle, *Ex-Reactor Transient Fission Gas Release Studies, Fuel Pin PNL-2-4*, HEDL TME 77-83, Hanford Engineering Development Laboratory, Richland, WA (May 1978).

21. H. H. Hummel, Physics of Reactor Safety, Quarterly Report, April-June 1975, ANL-75-67, p. 2.

22. W. C. Rivard and M. D. Torrey, *Numerical Calculation of Flashing from Long Pipes using a Two-Field Model*, Los Alamos Scientific Laboratory, LA-6104-MS (November 1975).

23. C. C. Miao, V. L. Shah, J. L. Krazinski and W. T. Sha, *Analytic Rebalance Technique for Pressure Calculation in Two-Phase Flow Systems*, NUREG/CR-1422, ANL-CT-80-19 (April 1980).

Distribution for NUREG/CR-1526 Vol. I (ANL-80-54 Vol. I)

Internal:

W. E. Massey
E. S. Beckjord
C. E. Till
J. B. Wozniak
R. Avery
P. B. Abramson
I. Bornstein/A. B. Klickman
C. E. Dickerman
F. E. Dunn
D. Ferguson/L. Baker
S. H. Fistedis
P. L. Garner
E. Gelbard
H. Henryson
H. H. Hummel (3)
I. T. Hwang/W. W. Marr
Kalimullah
M. F. Kennedy
D. H. Lennox
P. Pizzica
F. G. Prohammer
D. Rose/A. J. Goldman/
J. F. Marchaterre
R. Sevy
J. J. Sienicki
W. J. Sturm
B. J. Toppel
J. B. van Erp
D. Weber
H. Wider
H. M. Domanus
V. L. Shah
B. C-J. Chen
W. T. Sha
L. G. LeSage
P. I. Amundson/S. G. Carpenter
M. J. Lineberry
D. H. Shaftman
A. Travelli
ANL Contract File
ANL Libraries (3)
TIS Files (3)

External:

USNRC, Washington, for distribution per R7 (380)
DOE-TIC, Oak Ridge (2)
Manager, Chicago Operations and Regional Office, DOE
Chief, Office of Patent Counsel, DOE-CORO
President, Argonne Universities Association, Argonne, Ill.
Applied Physics Division Review Committee:
P. W. Dickson, Jr., Westinghouse Electric Corp., 3300 Appel Road, Bethel Park, Pa. 15102
R. L. Hellens, Combustion Engineering, Inc., Windsor, Conn. 06095
K. D. Lathrop, Los Alamos Scientific Lab., P.O. Box 1663, Los Alamos, N.M. 87545
W. B. Loewenstein, Electric Power Research Inst., P.O. Box 10412, Palo Alto, Calif. 94303
R. F. Redmond, College of Engineering, The Ohio State Univ., 2070 Neil Ave., Columbus, O. 43210
R. Sher, Dept. Mechanical Eng., Stanford U., Stanford, Calif. 94305
D. B. Wehmeyer, The Detroit Edison Co., 2000 Second Ave., Detroit, Mich. 48226
Components Technology Division Review Committee:
D. Berg, Mellon Inst. of Sciences, Carnegie-Mellon U., Pittsburgh, Pa. 15213
F. W. Buckman, Consumers Power Co., 1945 Parnall Rd., Jackson, Mich. 49201
P. F. Cunniff, Dept. Mechanical Eng., U. Maryland, College Park, Md. 20742
C. H. Kruger, Jr., Dept. Mechanical Eng., Stanford U., Stanford, Calif. 94305
M. A. Schultz, Dept. Nuclear Eng., The Pennsylvania State U., University Park, Pa. 16802
A. Sesonske, Dept. Nuclear Eng., Purdue U., West Lafayette, Ind. 47906
Y. C. L. S. Wu, Energy Conversion Div., U. Tennessee Space Inst., Tullahoma, Tenn. 37388
C. Erdman, U. Virginia, Charlottesville, Va. 22904
K. O. Ott, Purdue U., West Lafayette, Ind. 47906
R. Lancet, Atomics International, P.O. Box 309, Canoga Park, Calif. 91304